JSAE 2023XXXX
SAE 2023-YY-YYYY

Investigation of Exhaust Particles on Different TEM Grids: a Comparison between Graphene Oxide and Silicon Nitride Grids

Salvatore Lagana, Romans Akifjevs, Antonino La Rocca, Alasdair Cairns
Department of Mechanical Materials and Manufacturing Engineering, University of Nottingham

Michael W. Fay
Nanoscale and Microscale Research Centre, University of Nottingham, UK

Kevin F. Webb
Optics & Photonics Research Group, Faculty of Engineering, University of Nottingham, UK

ABSTRACT

Two different TEM (Transmission Electron Microscopy) grids - graphene oxide (GO) and silicon nitride (SiN) - were used to capture the particulates emitted with the exhaust of a modern 1.0 L GDI (Gasoline Direct Injection) engine. One speed-load condition (1250 rpm – idle) was chosen to generate a nanometric particulate output in the sub-23 nm regime which has been traditionally difficult to analyse in terms of composition and morphology. The overall aim was to understand if additional benefits can be obtained by analysing the particles captured in the exhaust on a nanoporous silicon nitride grid compared to state-of-the-art graphene oxide grids. The behaviour of porous SiN support films was of interest since nanopores are present in the grid in the 20 nm regime and the material is thermally and dimensionally stable under high temperatures, allowing thermophoretic capture directly within the engine exhaust stream. In addition to nanostructural and morphological comparison, the elemental composition of the particles was also analysed by EDX (Energy Dispersive X-Ray). Particles were thermophoretically captured directly in the exhaust stream using a dedicated probe holding the grid. Because of their tiny 2 nm thickness, GO grids work well for studying particle nanostructure, however background noise from copper and carbon interferes with compositional analysis by EDX. In contrast, the silicon nitride grids enable particle observation without this background noise, providing an intriguing platform for the analysis of the suspended particles collected by the pores. Future research will concentrate on producing particles with graphitic areas to assess imaging advantages in terms of morphological and nanostructural examination. The two grids were similar in their particle capture within the engine, with close mean primary particle diameters using both: 13.5 ± 3.1 nm standard deviation (SD) on GO and 14.1 ± 2.6 nm SD on SiN. EDX analysis suggests SiN grids, as C-free substrates, are preferable to GO for determining the carbon load in captured particles. This investigation is part of a larger project focusing on decarbonised fuels, so a carbon-free support film is pivotal in understanding the nature and composition of the fine particles linked to the lubricant oil.

INTRODUCTION

Particulates are among the principal air pollutants with strong evidence of their negative health impact [1]. The estimated number of deaths that can be related to particulate exposure was around 4.2 million yearly [2]. The main consequences of particulate inhalation/ingestion are well-known to be lung and heart diseases [3, 4]. In addition, it is found that small nanoparticles, in the sub-23 nm regime, have less difficulty transiting the respiratory system, entering the bloodstream, and are detectable even in the brain [4, 5]. Besides these health aspects, black carbon, which is a component of this pollutant [6], makes for environmental relevance as it is also one of the primary global-warming agents after carbon dioxide and methane [7]. Abatement of these emissions is consequently of the highest importance. 26% of all particulate emissions are caused by the transport sector, from internal combustion engine vehicles (ICEVs). This issue is generally thought to be resolvable with the mass production and sale of electric vehicles (EVs) in the next decade [8]. However, as ICEVs are expected to be around for at least 25-30 years [9], the study and reduction of emissions generated as a by-product of combustion are vital to accelerate the progress towards cleaner air and mitigate climate change.

European regulations track this direction of trying to limit air pollution from vehicles on the road. Euro 5, exclusively applied to diesel engines, included PN

(particle number) and PM (particle mass) limitations [10]. Current Euro 6 extended these limitations to gasoline engines after it emerged that they have comparable emissions to diesel when using modern direct injection technology (GDI - Gasoline direct injection) [10]. The adoption of PN with a permissible level of no more than 6 x 10^{11} #/km was prompted by the tendency of the most modern, optimised combustion engines to cause the formation of numerous nanoparticles with extremely low mass even downstream of a particulate filter [11, 12]. In the count, Euro 6 involves only solid particles > 23 nm, due to the size detection limitation of the Particle Number Counters (PNCs) on which the European standard, the Particle Measurement Program (PMP), relies [13]. The commercially available PNCs used in research and for PMP are the Condensation Particle Counters (CPCs) [14]. They need to be calibrated to the standard detection efficiency for their measurement to be acceptable. Over the last few years, the PMP has defined this standard as d50 = 23 nm and d90 = 41 nm, also denominated as "SPN23", to accommodate the detection size constraints of these instruments [15]. Another reason why the size range > 23 nm was chosen was to improve overall measurement repeatability by excluding unstable volatiles in the count [15, 16]. Solid particles < 23 nm are emitted in large quantities, - as a considerable amount of evidence suggests [17, 18] – and technological improvements to measure down to 10 nm have also been recently achieved [19]. Therefore, the newly proposed European regulation, Euro 7, which will be active from 2025 onwards, will also include solid particles > 10 nm in the 6 x 10^{11} #/km count [20]. The new method to comprise sub-23 nm particles will require a detection efficiency of d65±15 = 10nm and d90 = 15 nm (SPN10) [21] with the addition of a catalytic stripper (CS) to eliminate the volatiles. An alternative measuring device besides the CPC used to observe the solid particle number (SPN) is a differential mobility spectrometer (DMS). One of the most widely utilised commercial versions is the Cambustion DMS500. This plots a particle size distribution (PSD) which then can be used to obtain the particle count [22]. Various research works showed compliance of DMS500 to CPCs with d50 = 23 nm and d90 = 41 nm detection efficiency with either lognormal fitting [22-25] or digital filtering [22, 23, 26]. Now, validation against the latest CPCs with SPN10 detection efficiency should be sought [27].

Although these techniques allow for assessing the PN emitted by an ICE, they do not provide information about what particles they are composed of, their nanostructure, composition or morphology. The reason why the latter three are fundamental is that they supply an understanding of where the particles are originating from and how they might be generated aiding the design of a suitable filter. Transmission electron microscopy (TEM) is central in fulfilling the need for these in-depth compositional and morphological details. This technology allows for visualising the particles, enabling the qualitative assessment of their morphological nature and size [28]. In addition, High-resolution TEM (HRTEM), permits us to observe more closely and identify the primary particles' nanostructure [29]. Complementary EDX (energy dispersive X-Ray) analysis can be performed with TEM instrumentation to determine the elemental composition of particles [30]. Generally, the overall procedure involves capturing the soot by thermophoresis on a grid (graphene oxide lacey carbon copper mesh grid) and then placing this under TEM [29]. This method was used extensively to investigate particles either from engine oil [31, 32], exhaust gas [33, 34], and diffusion flames [35, 36]. La Rocca et al. [37], for instance, used TEM to characterise particles extracted from the lubricating oil of a gasoline direct injection engine (GDI). Pfau et al. [38], again with HRTEM, showed various nanostructural types for particles captured in the exhaust of a GDI engine on a TEM grid. In most of the aforementioned works, by TEM imaging, it is possible to observe particles with core-shell construction with an outer amorphous layer of varying thicknesses. Furthermore, in [38] they also compared measured PSDs from the TEM grid and from a DMS500 with and without CS. The grid average primary particle diameter was around 3.7 - 4.7 nm, against the 10 - 11 nm of the DMS. The contrast can be expected as the DMS measures electric mobility diameters, while with the TEM the actual particle can be seen and, in this case, it was possible to study particles even smaller than 10 nm that would be neglected even under Euro 7. The graphene oxide (GO) grid is widely employed because of its extremely thin 2 nm substrate. However, this did not allow the observation in detail of the nanostructure of such sub-10 nm particles due to the background carbon noise, since these samples are amorphous on the amorphous grid structure. This paper attempts to address this limitation by use of a novel grid type with a different, non-C, material composition.

Silicon Nitride (SiN) grids have been commercially available for several years, and used with TEM for different applications, for example for micro-organism detection [39] and for the analysis of plasmonic nanoparticles [40]. Capture for particles originating from combustion was also carried out in recent years with flame-generated samples [30, 41]. Many advantages are expected in utilising the SiN grids to analyse the post-combustion particles. First, they contain no carbon, therefore, EDX can immediately ensure that all carbon detected is effectively from the particles and not from the underlying grids. Also, these grids can have various pores of the size that can be tailored, which allow the visualisation of particles through voids, without either carbon or any other background disturbance. This should help to obtain a much clearer image if particles are trapped on top of these pores. Another advantage conferred by silicon nitride grids is the tuneable substrate thickness, reported between 20 nm to 300 nm for silicon nitride – the current grids being ~20 nm in thickness - [42] compared with less than 3 nm for lacey graphene oxide [43]. This can help the material be more resistant to harsh environments, allowing longer residency times in the exhaust stream for particulate capture. The scope of this paper is to verify the technical benefits of the SiN grid with respect to a carbon-based

(graphene oxide lacey carbon copper mesh) grid, which as seen from the above literature, is currently the most popular. Particles from the exhaust of a GDI engine will be captured with the two grids at the same operating condition, then these will be compared to each other under TEM with EDX.

METHODOLOGY

A Froude Consine EC38 TA Eddy-Current dynamometer with 154 kW of rated power was utilised to operate a three-cylinder 1L GDI engine. **Table 1**Table *1.* Engine specification. summarises the specifications of the engine. This was initially warmed up at mid-speed and mid-load of 1750 rpm – 20 Nm for about 20 – 30 minutes until the oil temperature reached 85 °C. Subsequently, the engine was ramped to a new steady-state condition of 1250 rpm – idle, which was run until oil temperature stability (change within 1-2 °C). These conditions were selected to collect exhaust particles because preliminary research showed that it was possible to successfully capture sub 23 nm on a TEM grid at a concentration suitable for surface analysis. In future work, it would be of interest to observe more conditions, although for this specific study one condition was deemed sufficient for the comparison of the two grids' capabilities. The rig arrangement is depicted in **Fig. 1**, showing that the location of the probe holding the TEM grid is situated within the exhaust pipe just after the turbo. This position was chosen to prevent excessive particle losses that usually occur along the pipe, and to maximise particle capture by thermophoresis. Each TEM grid, one SiN and one lacey GO, was held in turn for 3 minutes in the exhaust. This time restriction was necessary as it was found in previous work [38] that degradation of the lacey graphene oxide grid substrate can occur if it is held for longer. SiN grids are thermally stable at much higher temperatures and can be kept for extended durations [44]. In the preparation work, 3-, 5- and 10-minute exposure times were trialled with the SiN grid, but no advantage was observed in terms of concentration, likely because more oxidation occurred and as the grid holder temperature increased, the thermophoretic gradient decreased. Although oxidation is practically difficult to prevent, exposure time of 3 minutes was found to be an acceptable balance for sufficient concentration. Particle agglomeration takes place on the grid, but this does not affect the TEM analysis since the tool can visualise structure at the primary particle level. Captured particles were then investigated by HRTEM using a JEOL 2100F TEM in the Nanoscale and Microscale Research Centre (nmRC) at the University of Nottingham. An incident electron beam with a voltage of 250kV and various magnifications up to 250,000x were employed. A Gatan K3 was used for image acquisition. Furthermore, EDX could be performed with the use of the available X-MaxN 80 T. From the images collected, fringe analysis (method developed by Yehliu et al. [45] and described in detail by Pfau et al. [46]), and EDX was used to compare the two grids qualitatively. Aztec software was used to make the elemental maps.

Table 1. Engine specification.

Variable	Value
Max. Torque	170 Nm @ 1400 – 4500 rpm
Max. Power	92 kW @ 6000 rpm
Stroke	82.0 mm
Bore	71.9 mm
Compression Ratio (CR)	10.5:1
Volume	999 cm^3
Injector	5-hole solenoid
Max. Injection Pressure	200 bar (common rail)

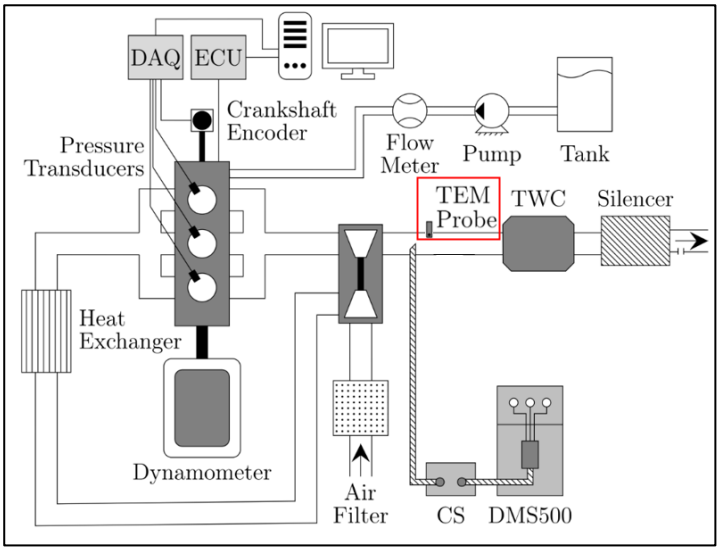

Fig. 1. Test rig set-up schematic.

RESULTS AND DISCUSSION

NANOSTRUCTURE ANALYSIS

In the following section images collected from HRTEM and are shown with their analysis. The images in **Fig. 2** serve to highlight key differences in analytics using the two types of TEM grids. The trapped soot agglomerate, shown in **Fig. 2 (A)**, sits on a thin layer of graphene oxide sheet. The differences in greyscale intensities across the particulate represent its dimensions in the z-axis, as further seen by variance in image focus in **Fig. 2 (B)**. Here, the agglomerate appears to be composed of approximately five individual primary particles. Each particle appears globular, with a central core surrounded by a semi-amorphous shell. The clarity of carbon fringes in this agglomerate is obstructed, partially due to overlapping of the particles and partially due to the amorphous background noise of the graphene oxide substrate. Inspection of **Fig. 2** (C) shows improved contrast. A soot agglomerate can be seen trapped on the silicon nitride surface, surrounded by a network of pores, acting as vacuum through-holes. The difference in grayscale intensity here is thought to be due to the unobstructed beam-path through the open pores. The thermally fabricated pores are polydisperse [47]. Some appear to be clouded over by material, which may suggest that a thin layer of substrate remains present over the pores. The higher magnification photo in **Fig. 2** (D) shows the soot fractal to be larger, and generally consisting of smaller globular primary particles, than its graphene oxide counterpart. Once again, the difference is fringe contrast and focus indicates varying volume and depth, as a known limitation of 2D HRTEM analysis [48]. However, a section of the agglomerate is positioned directly over the nanopore. Its globular nature and consistent grayscale intensity suggest it to be an individual amorphous primary carbon particle. This particle is not obstructed by the thick silicon nitride substrate, effectively suspended over vacuum, meaning the carbon fringes are clearly visible. MATLAB® fringe analysis in this section has been attempted, as developed by Yehliu et al. [45]. Pfau et al. state in their previous work [46] that the primary step in fringe analysis is the enhancement of contrast between fringes and the background, by employing histogram equalization which expands the distribution of colour intensities. It is important to note that for analysis over a nanopore, as seen in **Fig. 2** (D), this step may be unnecessary. Pfau et al. [46] observed both amorphous and graphitic domains at other higher speed and load conditions. By contrast, it was found that the particles in this study were typically heavily amorphous. This is because particle formation and nanostructure are affected by engine conditions. As a result, rather than being a definitive comparison, this nanostructure segment is still in progress. Further work is desirable to compare the effectiveness of MATLAB® fringe analysis across the two TEM grid types, under conditions where more graphitic particles are formed. Still, the presence of so many amorphous particles at fast-idle for this GDI is an interesting finding, since these present more reactive sites and therefore may be more easily oxidised and may impact on their adsorbed contaminant load [49, 50].

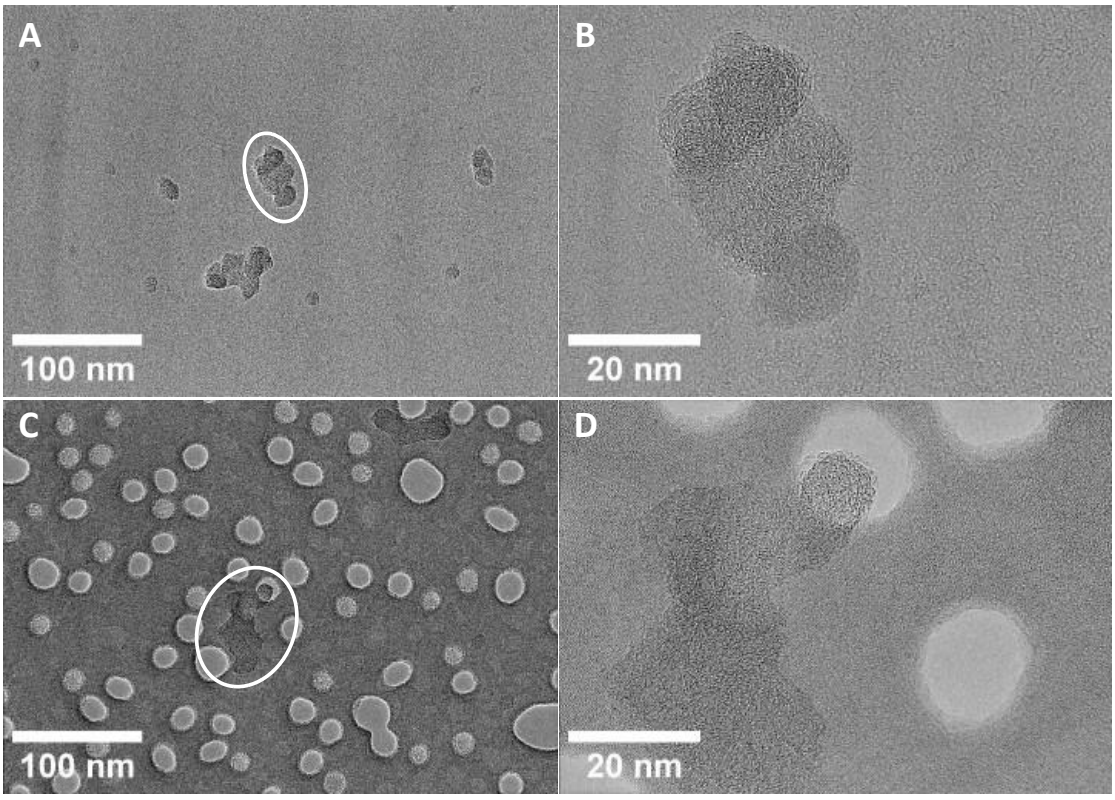

Fig. 2. TEM images of a soot agglomerate captured thermophoretically directly from the engine exhaust gas, at 1250rpm – idle, onto A-B) a conventional lacey graphene oxide grid, C-D) nanoporous silicon nitride nanomembrane grid. Trapped soot agglomerates are circled for convenience in A, C.

MORPHOLOGY ANALYSIS

Particles were measured by identifying soot agglomerates on the grid surface that had a skeleton-like structure, similar to **Fig. 2 (C)**. These agglomerates were more likely to contain individual globular primary particles towards the edges, as opposed to clusters as seen in **Fig. 2 (A)**, making it easier to identify and measure their diameter without overlapping and defocused features. The agglomerates selected appeared stable under the HRTEM beam, yielding no deformation or contamination, suggesting a lack of volatility. Across both types of substrates in this work, a relatively low concentration of soot agglomerates was observed. This may be due to the use of the gasoline GDI engine, which is conventionally considered relatively low in terms of emissions. Although grid exposure time in sampling channel was kept constant at three minutes for consistency, it may be possible in the future to increase the concentration of captured particles on the silicon grids by increasing the exposure time, since literature suggests this material is produced under and can therefore withstand high temperatures and pressures [42, 51, 52]. This also means that silicon grids could be used for more versatile studies in the future, such as, for example, assessing for oil combustion in particularly hot operating conditions, or monitoring if a sudden lack of coolant access has a significant impact on emissions.

Morphology analysis was performed using mostly 50kx magnification images, however 250kx images were used where appropriate to minimise measurement error. The particle sizing distributions in **Fig. 3** show individual data sets for primary particles assessed on both the lacey GO and SiN grids. For lacey GO, a total of 78 particles were identified across 20 images, taken from 3 separate tested grids. The mean primary particle diameter for this data was 13.5 nm, with a standard deviation of 3.1 nm and a median of 12.9 nm. The largest particle mode is at 11.5 nm, followed closely by 12.5 nm. Evaluation of the SiN grid was performed on 71 primary particles across 18 HRTEM images, taken from 2 grids. Mean primary particle diameter was measured at 14.1 nm, with an even lower standard deviation of 2.6 nm and a median of 13.5 nm. Here, the largest particle diameter mode is at 12.5 nm. Both data sets show good agreement, with a Gaussian fitting around the mean mode and decreasing particle counts towards both extremes. Both data sets showcase a predominant mode of sub-23 nm primary particles, suggesting great potential of using silicon nitride grids for this type of analysis. The measurement error between the two data sets falls within the expected range for a single comparison.

Previous work on GDI [38] at higher speeds and loads identified a distinct mode of sub-10 nm particles using a similar approach, reporting average diameters between 3.7 nm and 4.7 nm. The carbon grids in this work also did not show a distinct presence of sub-10 nm particles, despite a lack of pores for particles to pass through, which may suggest that this was mainly due to the operating condition, rather than the grid. In future work, the SiN could be designed with narrower nanopores even to trap and study exclusively sub-10 nm particles generated at those conditions [38], to evaluate their effect on human health [3]. This data shows a predominance of sub-23 nm particles that are under heavier scrutiny with the introduction of Euro 7. Overall, both grids can be deemed effective to investigate morphology, while the presence of nanopores in the silicon nitride grids, coupled with their carbon-free composition, present compelling advantages to future studies. This workflow can therefore be used as a complementary analysis when studying particle size distribution with other measuring devices (i.e. DMS500) [38].

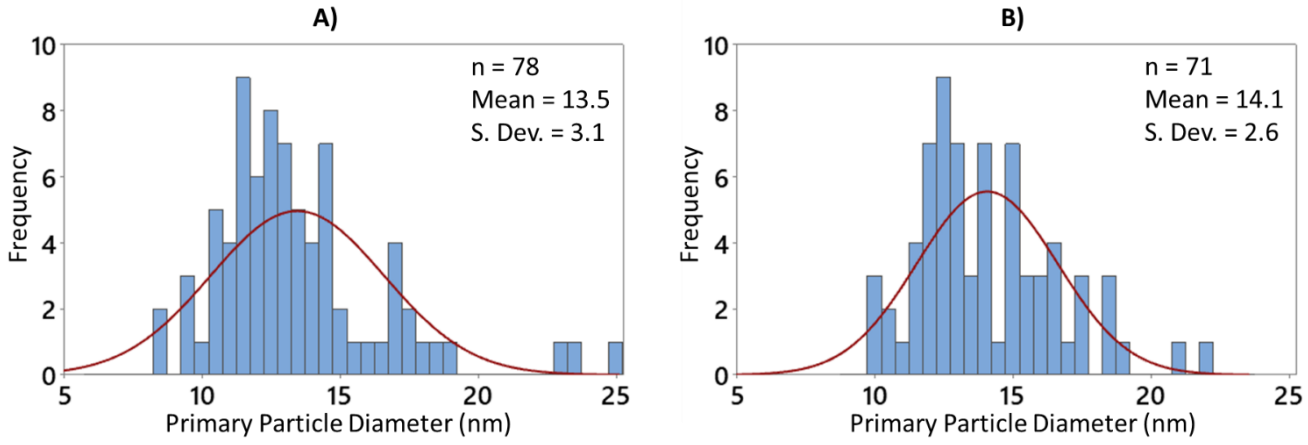

Fig. 3. Histogram plots showing primary particle sizing distribution using analysis of HRTEM images, sampled for three minutes at 1250rpm – idle, on A) lacey GO substrate, B) SiN substrate.

ENERGY DISPERSIVE X-RAY (EDX) SPECTROSCOPY ANALYSIS

Previous work [38] stated that EDX was attempted on GO grids, but proved inconclusive, likely due to copper sputtering from the copper mesh underlying the amorphous carbon and graphene oxide sheets. In this study, EDX was performed across both types of grids, to directly compare the results from matching particles and operating conditions, across different substrates.

Both types of grids had several regions of interest selected to contain one or more large soot agglomerate in the centre. In the case of lacey graphene oxide, these sites were selected centrally in the grid, to maximise the distance from both the copper grid and amorphous carbon mesh to the soot particulate. This was to minimise the chance of copper sputtering and background carbon signal from the grid. In the case of the silicon nitride grids, sites were preferentially selected to partially contain an agglomerate positioned over one or more nanopores. This was to assess stability of X-ray beam over particles suspended over vacuum, and to quantitively compare the obtained data against signal collected over the substrate material. Other experimental properties, including targeted volume of soot agglomerate, as well as EDX map scan time, vacuum and beam settings, were kept constant. Both map scans discussed in this work were taken over a duration of one hour, to maximise the chances of picking up surface elements present in very low concentrations. The data in **Fig. 4** shows the direct comparison of EDX data harvested across the two types of grids. The electron image in **Fig. 4 (A)** depicts a large, cluster-like structure, composed of primary carbon particles, trapped on a graphene oxide sheet. The carbon map in **Fig. 4 (B)** highlights that the soot agglomerate can be identified, however the surrounding area also creates strong carbon signal. This may be due to the graphene oxide sheets themselves, and relative intensity likely depends on thickness of sheet at that location. Furthermore, the elemental distribution in **Fig. 4 (C)** indicates that the predominant signal comes from copper at 78.7 Wt %, which agrees with copper sputtering reported in the past [38], despite efforts to maximise distance from the copper mesh. Total fraction of carbon in this scan is 17.9 Wt %, which does not give any quantifiable data without a means to distinguish soot agglomerate from the graphene oxide and amorphous carbon background. Obviously, this effect increases if EDX is used for longer as more counts are made. This is not optimal when small-percentage elements are also sought in the analysis. An example of this is sample in **Fig. 4 (D-F)** where 1 hour exposure increased substrate disturbance. The agglomerate in **Fig. 4 (G)** has a long chain-like structure. It is possible to see in the electron image also the location of the nanopores relative to the agglomerate. The particulate visibly covers several pores. The map scan in **Fig. 4 (H)** shows a clear outline of the agglomerate. It does not appear to vary with the presence of nanopores, and visibility only differs in intensity similarly to the electron image, higher saturation implying larger volume. Interestingly, the substrate surrounding this agglomerate is free of carbon signal (yellow) showing very clear distinction between the soot particulate and the substrate material. Furthermore, the relative presence of soot in this region of interest can be quantified, as seen in **Fig. 4 (I)**. The total fraction of carbon in this scan is 4.4 Wt % and can be reasonably attributed completely to soot, except for any other possible source of organic contaminant. The remaining majority is made up of 59.3 Wt % silicon and 27.3 Wt % nitrogen, as the two main constituents of the grid substrate. These EDX were collected for 5 more particles on SiN grids and all of them had C weight percentage detected from 2.5% to 6.7%, while in those 2 ones taken on GO grid, the wt% never went below 17%, confirming the graphene substrate disturbances. The entire elemental spectrum of the three particles from **Fig. 4** is depicted in **Fig. 5**. Other elements picked up during EDX across the two grids included iron, cobalt and chromium, which are all commonly due to scatter from the microscope polepiece. Gold was detected and this comes from the TEM holder. A large portion of the remaining elements was oxygen, and this is expected in both cases due to oxidation of soot inside the cylinder and along the tailpipe. A small fraction of silicon was detected on the graphene oxide grid; however, it is seen that silicon is a common polymer constituent for manufacturing TEM grids. Other unexpected elements included calcium and chlorine. Whilst calcium could be sourced from the combustion of engine lubricants, or simple contamination, the presence of chlorine is currently not understood. Chlorine was present in every SiN grid elemental analysis, indicating a manufacturing impurity that can be removed by plasma cleaning (which was not here attempted). The detection of these elements in combustion engine emissions shows the importance of the success of this work and the need for continued development of *ex-situ* analysis of seemingly clean exhaust gas.

The data in **Fig. 6** uses a layered EDX scan map of silicon and carbon to distinguish the grid substrate from nanopores, relative to the position of the soot agglomerate. The intensity of carbon signal (yellow) appears uniform across the substrate and the pores alike. It can further be inferred from this that the presence of nanopores underneath carbon particulates does not impact the obtained elemental data of carbon. This is a further advantage that promotes the use of silicon nitride grids in the context of exhaust evaluation as the quality of elemental spectrum data does not depend on positioning of the trapped agglomerate on the surface, and can be reliably performed on any chosen agglomerate.

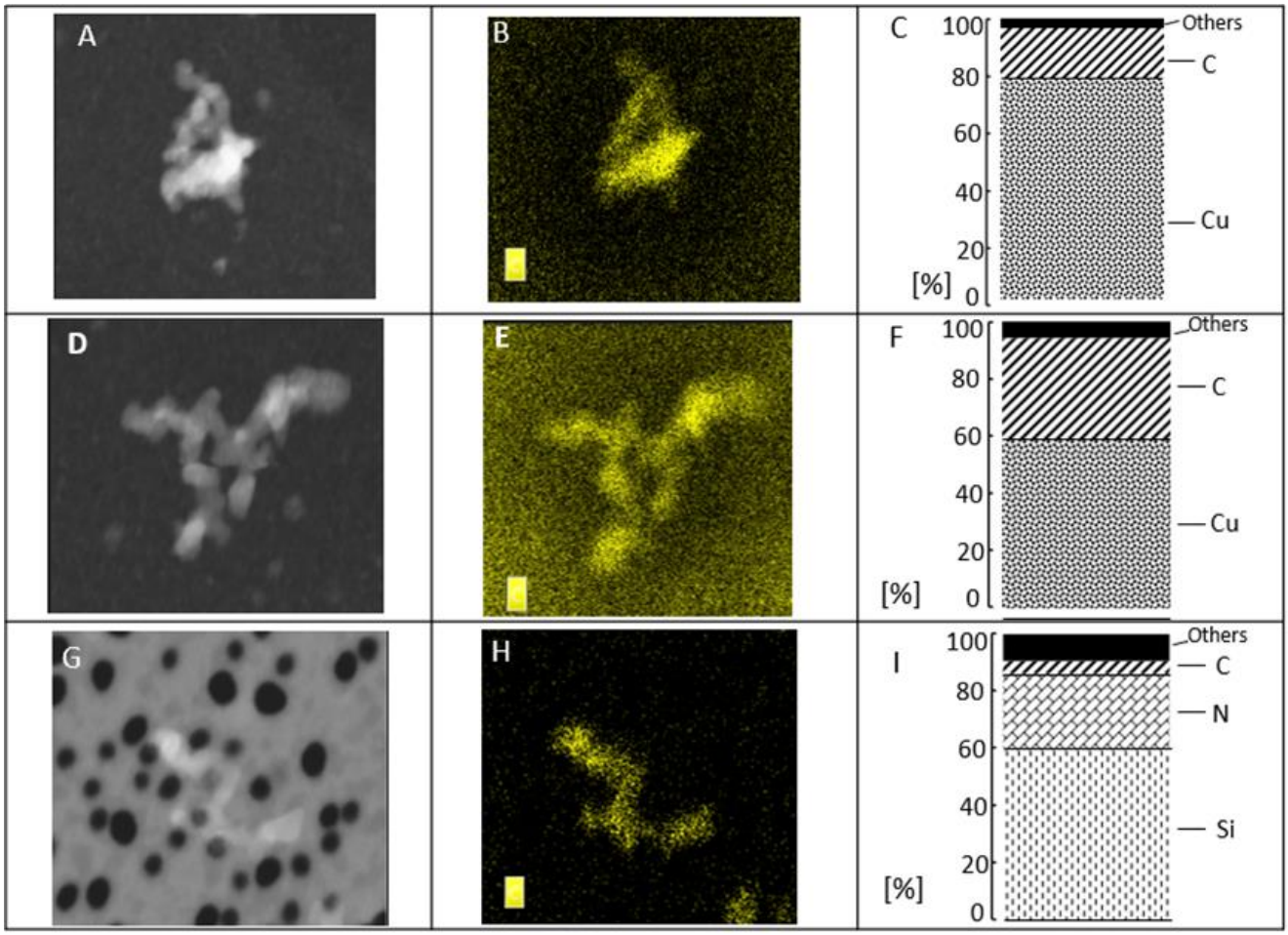

Fig. 4: EDX mapped data: A-C) GO grid 10-15min; D-F) GO grid 1 hour; G-I) SiN grid 10-15mins. A,D,G) EDX electron images of map scan areas. B,E,H) EDX maps showing localised intensities of carbon. C,F,I) Stacked column charts showing the absolute elemental distribution in map scans, by weight percentage.

Fig. 5: EDX spectra of GO particle 10-15 mins A), GO 1 hour B), and of SiN 10-15mins C) from Fig. 4.

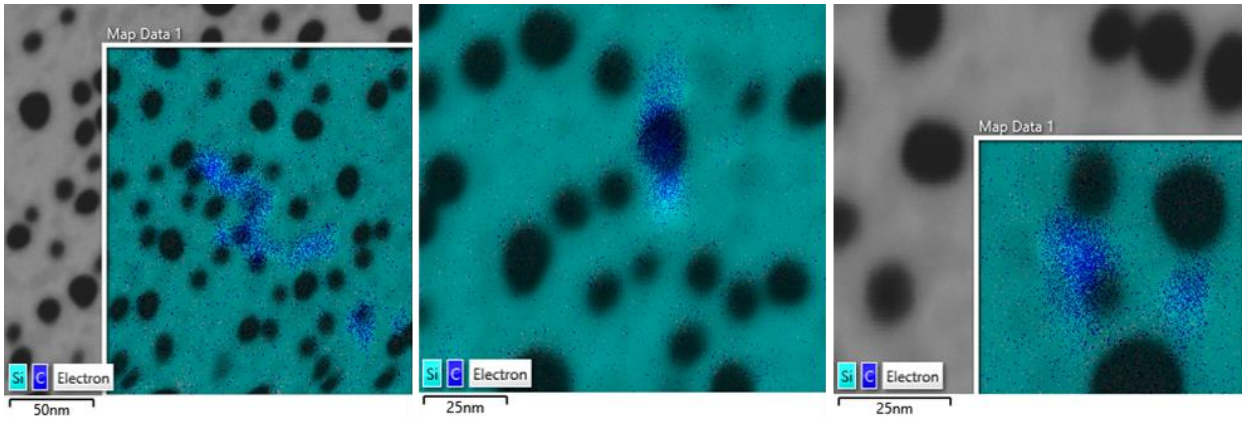

- Fig. 6. Layered images, showing several regions of interest, with EDX mapping of carbon and silicon overlayed with electron images, showing topology. Regions are displayed in order of decreasing EDX map scan size.

CONCLUSIONS

Graphene oxide (GO) and silicon nitride (SiN) TEM grids were used to capture particles emitted in the exhaust of a 1.0L GDI engine at a fixed speed and load condition (1250 rpm – idle). Nanostructure, morphology and EDX analysis were performed to observe difference in results between the two grids. The main findings were:

- Nanostructure of particles in both grids was predominantly amorphous. Fringes of particles on the nanopores of the SiN grid seemed much clearer with vacuum background. Benefits of this could not be quantified because not sufficient particles with graphitic carbon were found at this condition. Future work will focus on this quantification too.
- Morphological investigation showed similar primary particle size on both grids, which is expected as the particles are generated at the same condition. In GO grid, the mean primary particle diameter for this data was 13.5 nm, with a standard deviation of 3.1 nm and a median of 12.9. Using the SiN grids, mean primary particle diameter was measured at 14.1 nm, with a standard deviation of 2.6 nm and a median of 13.5 nm. This means that this type of study can be compared between grid types.
- EDX on GO grid allows the observation of particulates and elements produced by engine combustion, but the carbon background from the substrate biases the amount coming from the particles. By comparison, the SiN grid more accurately quantifies the carbon from the particle, since the C-free substrate is mainly silicon and nitrogen. Also, any location on the SiN grid is viable to study elemental analysis, while the GO grids must be used away from the copper mesh and from the lacey carbon film.

In conclusion, this paper shows the SiN grid is as viable as commonly used lacey GO to study particles generated from an internal combustion engine exhaust. Fringe analysis should be evaluated in future work with more graphitic particles because it is expected that nanopores may benefit this analysis. Morphology can be studied equally on both, while EDX seems to be more favourable on SiN grid due to the absence of carbon in the background. This characteristic is expected to be crucial when studying emissions from decarbonised fuels engines in the future to assess with certainty that carbon is coming from the oils.

ACKNOWLEDGEMENTS

The authors thank John Lane and Nigel Sykes for technical support with the engine setup. The authors also thank the Nanoscale and Microscale Research Centre (nmRC), supported by the Engineering and Physical Sciences Research Council (EPSRC) [under grant EP/W006413/1] and the University of Nottingham, for providing access to instrumentation. In addition, thanks to Prof James McGrath, University of Rochester, NY and SiMPore Inc, Rochester, NY for making available the 20nm NPN chips for evaluation. This work was supported by the Engineering and Physical Sciences Research Council through the scholarship provided by EPSRC for Salvatore Lagana [grant number EP/T517902/1].

AUTHORS CONTRIBUTIONS

Conceptualization, S.L.; Methodology, S.L.; Software, S.L., R.A.; Investigation, S.L., R.A; Data Curation, S.L., R.A, M.F.; Formal analysis, S.L., R.A.; Validation, S.L., R.A; Visualization, S.L., R.A, M.F.; Writing - Original Draft, S.L., R.A; Writing - review & editing S.L., R.A, A.L.R.; Supervision, A.L.R., A.C., K.W.; Funding acquisition, A.L.R., A.C. All authors have read and agreed to the published version of the manuscript.

REFERENCES

1. World Health Organization. *Ambient (outdoor) air pollution*. 2022 [cited 2023 n.d.]; Available from: https://www.who.int/news-room/fact-sheets/detail/ambient-(outdoor)-air-quality-and-health.

2. World Health Organization, *Ambient air pollution: a global assessment of exposure and burden of disease*. 2016, Geneva: World Health Organization.

3. Du, Y., et al., *Air particulate matter and cardiovascular disease: the epidemiological, biomedical and clinical evidence.* J Thorac Dis., 2016. **8**(1): p. E8-E19.

4. US Environmental Protection Agency. *Health and Environmental Effects of Particulate Matter (PM)*. 2022 [cited n.d. October 04, 2022]; Available from: https://www.epa.gov/pm-pollution/health-and-environmental-effects-particulate-matter-pm.

5. Oberdörster, G., et al., *Translocation of inhaled ultrafine particles to the brain.* Inhal Toxicol, 2004. **16**(6-7): p. 437-45.

6. Climate and Clean Air Coalition. *Climate and Clean Air Coalition (CCAC) - Black carbon*. 2022 [cited n.d. October 04, 2022]; Available from: https://www.ccacoalition.org/en/slcps/black-carbon.

7. Stocker, T.F., et al., *Climate Change 2013: The Physical Science Basis. Contribution of Working Group I to the Fifth Assessment Report of the Intergovernmental Panel on Climate Change*. 2013, IPCC: Cambridge, United Kingdom and New York, NY, USA, . p. 1535.

8. Evadoption. *EV Sales Forecasts*. 2023 [cited 2023 n.d.]; Available from: https://evadoption.com/ev-sales/ev-sales-forecasts/.

9. Krajinska, A., *Euro 7: Europe's chance to have clean air*. 2021, Transport and Environment.

10. Williams, M. and R. Minjares, *A technical summary of Euro 6/VI vehicle emission standards*, in *International Council on Clean Transportation (ICCT)*. 2016.

11. Burtscher, H.M., W. E., *Particulate Measurements*, in *DieselNet*. 2012.

12. Burtscher, H., *Physical characterization of particulate emissions from diesel engines: a review.* Journal of Aerosol Science, 2005. **36**(7): p. 896-932.

13. Unece. *ECE/TRANS/WP.29/GRPE/*. 2020 [cited n.d. November 08, 2022]; Available from: http://www.unece.org/trans/main/wp29/wp29wgs/wp29grpe/grpeage.html.

14. European Commission, et al., *Particle Measurement Programme (PMP) : inter-laboratory correlation exercise with condensation particle counters (CPCs)*. 2019: Publications Office.

15. Giechaskiel, B., et al., *Measurement of Automotive Nonvolatile Particle Number Emissions within the European Legislative Framework: A Review.* Aerosol Science and Technology, 2012. **46**(7): p. 719-749.

16. Mathis, U., et al., *Sampling Conditions for the Measurement of Nucleation Mode Particles in the Exhaust of a Diesel Vehicle.* Aerosol Science and Technology, 2004. **38**(12): p. 1149-1160.

17. Giechaskiel, B., *Differences between tailpipe and dilution tunnel sub-23 nm nonvolatile (solid) particle number measurements.* Aerosol Science and Technology, 2019. **53**(9): p. 1012-1022.

18. Giechaskiel, B., et al. *European Regulatory Framework and Particulate Matter Emissions of Gasoline Light-Duty Vehicles: A Review*. Catalysts, 2019. **9**, DOI: 10.3390/catal9070586.

19. Samaras, Z., et al., *Perspectives for regulating 10 nm particle number emissions based on novel measurement methodologies.* Journal of Aerosol Science, 2022. **162**: p. 105957.

20. Gospodinova, S. and F. Miccoli. *Commission proposes new Euro 7 standards to reduce pollutant emissions from vehicles and improve air quality*. 2022 [cited n.d. Dec 21, 2022]; Available from:

https://ec.europa.eu/commission/presscorner/detail/en/ip_22_6495.

21. Lähde, T., et al., *Solid particle number emissions of 56 light-duty Euro 5 and Euro 6 vehicles.* Journal of Aerosol Science, 2022. **159**: p. 105873.

22. Leach, F., *Particulate emissions from gasoline direct injection engines*. 2014, Oxford University, UK.

23. Symonds, J., *Catalytic Stripper Accessory (CSA) for the DMS500 for sub 23 nm particles (or above)*. 2020.

24. Leach, F., et al., *Predicting the particulate matter emissions from spray-guided gasoline direct-injection spark ignition engines.* Proceedings of the Institution of Mechanical Engineers, Part D: Journal of Automobile Engineering, 2016. **231**(6): p. 717-730.

25. Braisher, M., R. Stone, and P. Price, *Particle Number Emissions from a Range of European Vehicles*, in *SAE 2010 World Congress & Exhibition*. 2010, SAE International.

26. Leach, F.C.P., et al., *The effect of oxygenate fuels on PN emissions from a highly boosted GDI engine.* Fuel, 2018. **225**: p. 277-286.

27. Leach, F., et al., *Sub-23 nm Particulate Emissions from a Highly Boosted GDI Engine*, in *14th International Conference on Engines & Vehicles*. 2019, SAE International.

28. Pósfai, M. and P.R. Buseck, *Nature and Climate Effects of Individual Tropospheric Aerosol Particles.* Annual Review of Earth and Planetary Sciences, 2010. **38**(1): p. 17-43.

29. Pfau, S.A., *Nanoscale characterisation of soot particulates from gasoline direct injection engines*. 2021, University of Nottingham, UK.

30. Chen, C., et al. *The Impact of Sampling Medium and Environment on Particle Morphology*. Atmosphere, 2017. **8**, DOI: 10.3390/atmos8090162.

31. Uy, D., et al., *Characterization of gasoline soot and comparison to diesel soot: Morphology, chemistry, and wear.* Tribology International, 2014. **80**: p. 198-209.

32. La Rocca, A., et al., *The nanostructure of soot-in-oil particles and agglomerates from an automotive diesel engine.* Tribology International, 2013. **61**: p. 80-87.

33. Liati, A., et al., *Electron microscopic characterization of soot particulate matter emitted by modern direct injection gasoline engines.* Combustion and Flame, 2016. **166**: p. 307-315.

34. Barone, T.L., et al., *An analysis of direct-injection spark-ignition (DISI) soot morphology.* Atmospheric Environment, 2012. **49**: p. 268-274.

35. Alfè, M., et al., *Structure–property relationship in nanostructures of young and mature soot in premixed flames.* Proceedings of the Combustion Institute, 2009. **32**(1): p. 697-704.

36. Apicella, B., et al., *Soot nanostructure evolution in premixed flames by High Resolution Electron Transmission Microscopy (HRTEM).* Proceedings of the Combustion Institute, 2015. **35**(2): p. 1895-1902.

37. La Rocca, A., et al., *Characterisation of soot in oil from a gasoline direct injection engine using Transmission Electron Microscopy.* Tribology International, 2015. **86**: p. 77-84.

38. Pfau, S.A., et al., *Linking operating conditions of a GDI engine to the nature and nanostructure of ultrafine soot particles.* Combustion and Flame, 2022. **245**: p. 112315.

39. Lausch, V., et al., *Silicon nitride grids are compatible with correlative negative staining electron microscopy and tip-enhanced Raman spectroscopy for use in the detection of micro-organisms.* Journal of Applied Microbiology, 2014. **116**(6): p. 1521-1530.

40. Mulligan, S.K., et al., *Multiplexed TEM Specimen Preparation and Analysis of Plasmonic Nanoparticles.* Microsc Microanal, 2015. **21**(4): p. 1017-1025.

41. Vargas, A.M., *Design and Development of a Thermophoretic Soot Sampling*

System for High-Pressure Laminar Diffusion Flames. 2016, University of Toronto, Canada.

42. Vlassiouk, I., et al., *Versatile ultrathin nanoporous silicon nitride membranes.* Proceedings of the National Academy of Sciences, 2009. **106**(50): p. 21039-21044.

43. ACS Material. *ACS Material Graphene on Lacey Carbon 300 Mesh Copper TEM Grids* 2012 [cited 2023 n.d.]; Available from: https://www.acsmaterial.com/pub/media/catalog/product/t/d/tds-graphene_on_lacey_carbon_300_mesh_copper_tem_grids.pdf.

44. Zhang, Z. and D. Su, *Behaviour of TEM metal grids during in-situ heating experiments.* Ultramicroscopy, 2009. **109**(6): p. 766-74.

45. Yehliu, K., R.L. Vander Wal, and A.L. Boehman, *Development of an HRTEM image analysis method to quantify carbon nanostructure.* Combustion and Flame, 2011. **158**(9): p. 1837-1851.

46. Pfau, S.A., A. La Rocca, and M.W. Fay, *Quantifying soot nanostructures: Importance of image processing parameters for lattice fringe analysis.* Combustion and Flame, 2020. **211**: p. 430-444.

47. Madejski, G., et al. *TEM Tomography of Pores with Application to Computational Nanoscale Flows in Nanoporous Silicon Nitride (NPN)*. Membranes, 2018. **8**, DOI: 10.3390/membranes8020026.

48. Khetrapal, A. *Limitations of TEM*. News Medical Life Sciences 2019 [cited 2023 n.d.]; Available from: https://www.news-medical.net/life-sciences/Limitations-of-TEM.aspx.

49. Gaddam, C.K., *Physical and Chemical Characterization of Gasoline Particulates and Differences Relative to Diesel Soot*. 2012, Pennsylvania State University, USA.

50. Yehliu, K., et al., *Impact of fuel formulation on the nanostructure and reactivity of diesel soot.* Combustion and Flame, 2012. **159**(12): p. 3597-3606.

51. Zhang, Z. and D. Su, *Behaviour of TEM metal grids during in-situ heating experiments.* Ultramicroscopy, 2009. **109**(6): p. 766-774.

52. DesOrmeaux, J.P.S., et al., *Nanoporous silicon nitride membranes fabricated from porous nanocrystalline silicon templates.* Nanoscale, 2014. **6**(18): p. 10798-10805.

DEFINITIONS, ACRONYMS ABBREVIATIONS

TEM: Transmission Electron Microscopy.

GO grid: Graphene Oxide grid.

SiN grid: Silicon Nitride grid.

GDI: Gasoline Direct Injection

EDX: Energy Dispersive X-Ray.

SD: Standard deviation.

ICEVs: Internal Combustion Engine Vehicles.

EVs: Electric Vehicles.

PN: Particle Number.

PM: Particle Mass.

PNCs: Particle Number Counters.

PMP: Particle Measurement Program.

CPCs: Condensation Particle Counters.

SPN: Solid Particle Number.

SPN23: Standard detection efficiency method counting “Solid Particle Number” with 50% efficiency at 23 nm and 90% at 41 nm. This currently used by PMP with Euro 6.

Sub-23 nm: Particles under 23 nm in diameter.

SPN10: New proposed standard detection efficiency method counting “Solid Particle Number” with 65±15% efficiency at 10 nm and 90% at 15 nm. In Euro 7 from 2025.

CS: Catalytic Stripper

DMS: Differential Mobility Spectrometer.

PSD: Particle Size Distribution.

HRTEM: High Resolution Transmission Electron Microscope